Factor Graph based Equalizer for Two Way Relaying Channels with General Waveforms

Matthias Woltering, Dirk Wübben, and Armin Dekorsy
University of Bremen, Bremen, Germany
Email: {woltering, wuebben, dekorsy}@ant.uni-bremen.de

***Abstract*—Multi-carrier schemes with general waveforms are flexible bandwidth efficient transmission schemes offering a robust design regarding practical impacts like carrier frequency offset and timing offsets. Especially for two phase two way relaying channels (TWRC) where two users simultaneously transmit data on the same resources, a robust design in presence of practical constraints is important. This paper focuses on the equalization at the relay with factor graph based techniques reducing the impact of the physical channels and offsets. The combination of general waveforms and factor graph based equalizers offers a flexible structure giving control of the complexity and FER performance at the relay. Hence, we fully describe a TWRC transmission by factor graphs for general multi-carrier transmissions, which gives us a framework on iterative detection of the relay message based on the sum-product algorithm. It turns out that well localized waveforms applying a factor graph based equalizer outperforms OFDM w.r.t. FER performance under practical constraints.**

I. Introduction

For the upcoming 5^{th} generation of mobile communication different waveform candidates are discussed aiming a high spectral efficiency and a flexible time-frequency resource allocation [1], [2]. To further increase the spectral efficiency an assisting relay helps to reduce the path loss and offer bi-directional communication between two users in Two Way Relay Channels (TWRCs) [3]–[7]. With two-phase TWRC two users can exchange information with each other without the drawback of any half-duplex constraint. Since many standards are using OFDM with Cyclic Prefix (CP), the combination of CP-OFDM and TWRC has been analyzed among others in [7]–[10]. However, in [11]–[14] it was shown that the combination suffers from individual channel phase terms and Carrier Frequency Offset (CFO) of each user, which cannot be resolved individually at the relay. In contrast to a Point-to-Point (P2P) transmission, where such impact can be estimated and pre-compensated at the receiver and the simple 1-tap equalizer for CP-OFDM can be used, in TWRC only a joint compensation is possible leading to severe Frame Error Rate (FER) performance degradations by this simple equalization scheme. Hence, the equalizer has to be able to deal with the impacts of the channels and the offsets. Sum Product Algorithm (SPA) working on factor graphs [15]–[17] can deal with influences directly in the equalization step at the receiver. This was analyzed for a P2P transmission in CP-OFDM assuming low time-variant channels in [18]. In [19], the factor graph based equalizer is analyzed under doubly-dispersive channels within MIMO-OFDM. The ideas of factor graph based equalization of doubly dispersive channels has been extended for TWRCs in [10].

The focus of this work is a configurable equalizer adapting the channel impact, where the complexity is controlled by a proper choice of Transmitter/Receiver (Tx/Rx) filters within multi-carrier schemes. The equalizer is based on factor graphs implementing the SPA. Especially in TWRC the impact of the channel, CFOs or Timing Offsets (TOs) cannot be compensated individually. Thus, a proper combination of waveform and equalization techniques is important.

To introduce the general ideas, we first present the system model of a P2P transmission in Subsection II-A including the impact of the physical channel with delay spread, Doppler shifts and additional offsets. Furthermore, general multi-carrier schemes utilizing well-localized Tx/Rx filters being more robust against practical impairments are presented and compared the traditional CP-OFDM with rectangular waveform and additional guard interval. In particular, the corresponding factor graphs are described in Subsection II-B for CP-OFDM and the general multi-carrier scheme QAM/Filter Bank Multi-Carrier (FBMC) (QAM/FBMC) applying non-orthogonal but well-localized Gaussian Tx/Rx filters. We further introduce the SPA for the equalizer serving as symbol-by-symbol Maximum A-Posteriori (MAP) detector in Subsection II-C and discuss the tradeoff between computational complexity and FER performance under practical constraints in Subsection II-D. Section III extends the idea of factor graphs in TWRC using general waveforms. Furthermore, it introduces a framework on a complete detection method at the relay based on factor graphs. Also, this section is concluded by link level simulations giving the FER performance at the relay. The last section concludes the paper and gives a short outlook on possible investigations in the future.

II. P2P transmission

A. System Model

Fig. 1 shows the block diagram of a P2P transmission, where a user information sequence vector $\mathbf{b} \in \mathbb{F}_2^{N_b}$ of length N_b is encoded by a binary linear encoding scheme to a coding sequence $\mathbf{c} \in \mathbb{F}_2^{N_c}$ of length N_c with code rate $R_\text{c} = N_b/N_c$. The modulation block $\mathcal{M}(\cdot)$ collects $\log_2(M)$ code bits and maps them to an M-ary complex symbol $d^{(k,\ell)}$ of a transmit frame matrix $\mathbf{D} \in \mathbb{C}^{N_k \times N_\ell}$ with N_k the number of sub-carriers and N_ℓ the number of time instances. By a general

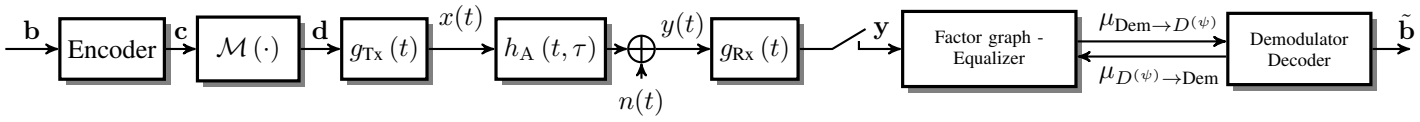

Fig. 1. Block diagram of a P2P transmission with a factor graph based equalizer at the receiver.

waveform

$$g_{\text{Tx}}^{(k,\ell)}(t) = g_{\text{Tx}}(t - \ell T)\, \mathrm{e}^{j2\pi kF}, \tag{1}$$

the complex symbol $d^{(k,\ell)}$ is shifted to a time-frequency point $(kF, \ell T)$ or shorter (k,ℓ), with sub-carrier spacing F and symbol spacing T.

In case of the multi-carrier scheme OFDM a rectangular Tx/Rx filter

$$g_{\text{Tx}}(t) = \begin{cases} 1/\sqrt{T} & -\frac{T}{2} \le t < \frac{T}{2} \\ 0 & \text{otherwise,} \end{cases} \tag{2}$$

is used. For the other general multi-carrier scheme used in this work, namely QAM/FBMC, more general waveforms are possible. Throughout this work, we concentrate on QAM/FBMC applying an isotropic Gaussian waveform with localization factor $\alpha = 1$ given by

$$g_{\text{Tx}}(t) = (1/\alpha)^{1/4} \mathrm{e}^{\alpha t^2} \quad . \tag{3}$$

At the receiver, matched filtering is applied and the signal is sampled with sampling time T yielding the overall system model

$$\mathbf{y} = \mathbf{V}\mathbf{d} + \mathbf{n} \quad . \tag{4}$$

The received signal vector $\mathbf{y} \in \mathbb{C}^{N_k N_\ell \times 1}$ is a stacked vector $\mathbf{y} = \mathrm{vec}\{\mathbf{Y}\}$, where the matrix $\mathbf{Y}$ can be interpreted as the sampled observations on receive time-frequency point (k', ℓ'). Similarly, the data symbol vector $\mathbf{d}$ is a stacked version of the matrix $\mathbf{D}$ introduced above. The noise vector $\mathbf{n}$ is complex circular Additive White Gaussian Noise (AWGN) with $\mathcal{N}\{0, \sigma_{\text{n}}^2\}$. As a shorthand notation, we use the received running index $\rho = k' + \ell' N_k$ and transmitted running index $\psi = k + \ell N_k$ for the vectors $\mathbf{y}$ and $\mathbf{d}$.

The impact of the used multi-carrier transmissions schemes and the influence of the channel can be described by the effective channel matrix $\mathbf{V} \in \mathbb{C}^{N_k N_\ell \times N_k N_\ell}$. Each element $v^{(\rho,\psi)} = f(H(\tau,\nu), g_{\text{Tx}}^{(\psi)}, g_{\text{Rx}}^{(\rho)})$ is a function of the used Tx/Rx filters in (2) or (3) and of the channel given in (5), it is described in detail in [20]–[22]. The physical channel in this work is a doubly dispersive channel given by the delay-Doppler function

$$H(\tau,\nu) = \sum_{\iota=0}^{N_{\text{h}}-1} h_\iota \delta(\tau - \tau_\iota - \Delta\tau)\, \delta(\nu - \nu_\iota - \Delta\nu). \tag{5}$$

Here, all influences of the channel, like the complex channel gain h_ι of a path ι, delay spread τ_ι, CFO $\Delta\nu$, Doppler spread ν_ι and TO $\Delta\tau$ are considered.

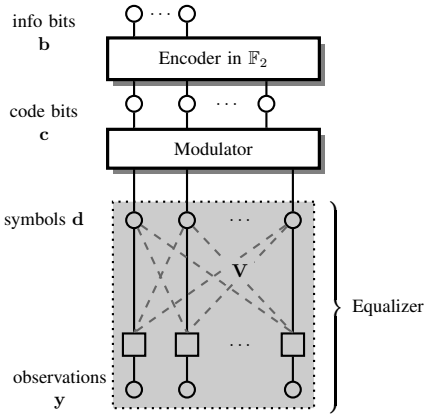

Fig. 2. Factor graph of the transmission. Edges between the symbol variable of user A and channel observations

The task at the receiver side is to estimate the data information sequence $\tilde{\mathbf{b}}$ based on the received signal vector $\mathbf{y}$, which is done by a MAP detection for each bit b_ζ given by

$$\tilde{b}_\zeta = \arg\max_{b_\zeta \in \mathbb{F}_2} p(b_\zeta|\mathbf{y}) \quad . \tag{6}$$

Within this work we consider the SPA algorithm [15], [17], [23] working on factor graphs. Note that, in P2P transmissions the compensation of CFO $\Delta\nu$ and TO $\Delta\tau$ can be done separately before equalization. However, here we focus on solving the impact within the equalizer. In contrast, the TWRC (introduced later) suffers, among other things, from CFO and TO which cannot be compensated individually due to the superposition of two users on the same resources. Thus, we first briefly explain factor graphs and the SPA algorithm in the P2P transmission and compare this technique within OFDM and QAM/FBMC with the standardized CP-OFDM using low-complexity 1-tap equalization. Then in Section III we extend the ideas to TWRC.

B. Factor Graph

According to [17], the MAP detector (6) can be factorized to

$$\tilde{b}_\zeta = \arg\max_{b_\zeta \in \mathbb{F}_2} \underbrace{p(\mathbf{y}|\mathbf{d})}_{\text{Equalizer}} \underbrace{p(\mathbf{d}|\mathbf{c})}_{\text{Modulator}} \underbrace{p(\mathbf{c}|b_\zeta)}_{\text{Encoder}} \underbrace{p(b_\zeta)}_{\text{a-priori}}. \tag{7}$$

The corresponding factor graph of the system in (4) is illustrated in Fig 2. Each block corresponds to a part of the right-hand-side in (7). The P2P demodulator and detector are out of scope of this work and for these State-of-the-Art algorithms are used.

To generate the factor graph of the equalizer the adjacency matrix $\mathbf{A}$ is defined, based on the elements $v^{(\rho,\psi)}$ of effective

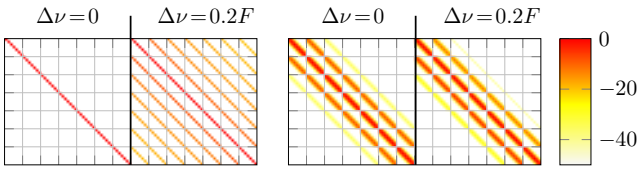

a) rectangular b) Gaussian

Fig. 3. Illustration of the effective matrix with $\Delta\nu = 0$ and $\Delta\nu = 0.2F$ in case of a rectangular and a Gaussian Tx/Rx filter.

channel matrix $\mathbf{V}$, like

$$[\mathbf{A}]_{\rho,\psi} = \begin{cases} 1 & , \ |\upsilon^{(\rho,\psi)}|^2 \geq \varepsilon \\ 0 & , \ \text{otherwise,} \end{cases} , \tag{8}$$

where only entries are set to 1 with a power $|\upsilon^{(\rho,\psi)}|^2$ larger than a threshold ε. The matrix $\mathbf{A}$ gives the edges between each variable $d^{(\psi)}$ and the corresponding $y^{(\rho)}$, if the element $[\mathbf{A}]_{\psi,\rho} = 1$. Furthermore, the number of connected edges to a variable node $N^{(d)}_{\text{edges}}(\psi)$ and the number of connection to a factor node $N^{(y)}_{\text{edges}}(\rho)$ can be calculated by

$$N^{(d)}_{\text{edges}}(\psi) = \sum_{j=0}^{N_k N_\ell - 1} [\mathbf{A}]_{\psi,j} \tag{9}$$

$$N^{(y)}_{\text{edges}}(\rho) = \sum_{i=0}^{N_k N_\ell - 1} [\mathbf{A}]_{i,\rho} \quad . \tag{10}$$

On each edge messages are exchanged from a factor to a variable node and vice versa. Therefore, the number of edges indicates the complexity of the SPA algorithm.

As an example Fig. 3 illustrates the effective channel matrix $\mathbf{V}$ using rectangular and Gaussian Tx/Rx filters for channels only affected by different CFOs with $\Delta\nu = 0$ and $\Delta\nu = 0.2F$. It can be observed, that the effective channel matrix of a rectangular Tx/Rx filter without a CFO is purely diagonal. Assuming $\varepsilon = 0$, the number of edges is $N^{(d)}_{\text{edges}}(\psi) = 1$ and $N^{(y)}_{\text{edges}}(\rho) = 1$, hence, only one variable is connected to one factor $y^{(\rho)} = \upsilon^{(\rho,\psi)} d^{(\psi)}$. In other words no interference occurs and a 1-tap equalizer is sufficient. However, with a CFO of $0.2F$, the number of edges increases dramatically. For this reason the complexity in the SPA will grow significantly. Although the Gaussian waveform will introduce some more edges in the ideal case, but the change between number of edges is small under the practical constraint like, e.g., a CFO as indicated on the right plot of Fig. 3 and the complexity stays similar.

The solid straight lines in Fig. 2 denote the direct connection of a symbol to a factor node with $\psi = \rho$, the dashed lines denote the interfering symbols. As indicated by (8), the adjacency matrix is generated based on the power of each channel coefficient $|\upsilon^{(\rho,\psi)}|^2 > \varepsilon$. Consequently, the effective channel matrix and the threshold ε control the amount of messages exchanged within the SPA as it will be discussed in the next part.

C. Sum Product Algorithm

The SPA is a formal description exchanging messages on the edges between variable nodes and factor nodes of a factor graphs like in Fig. 2. The calculation of a message from a factor node $Y^{(\rho)}$ to a variable node $D^{(\psi)}$ for the realization $d^{(\psi)}$ is given by

$$\mu_{Y^{(\rho)}\to D^{(\psi)}}\left(d^{(\psi)}\right) = \sum_{\sim\{d^{(\psi)}\}} p\left(y^{(\rho)}, \mathbf{d}\right) \prod_{\sim\{d^{(\psi)}\}} \mu_{D^{(\psi)}\to Y^{(\rho)}}\left(d^{(\psi)}\right) \tag{11}$$

The names of nodes are denoted with capital letter, the realizations with small letters and the notation is mainly based on [17]. The term $\sim\{d^{(\psi)}\}$ is a short hand notation for a set containing all elements connected to this node except $d^{(\psi)}$ given by the adjacency matrix. The message $\mu_{Y^{(\rho)}\to D^{(\psi)}}\left(d^{(\psi)}\right)$ of the factor $Y^{(\rho)}$ to the variable node $D^{(\psi)}$ is performing the marginalization over the likelihood function:

$$p\left(y^{(\rho)}, \mathbf{d}\right) \propto \exp\left(-\frac{1}{\tilde{\sigma}^2_{\text{n},\kappa}} \left| y^{(\rho)} - \sum_{\psi} \upsilon^{(\rho,\psi)} d_\psi \right|^2\right) . \tag{12}$$

The noise term $\tilde{\sigma}^2_{\text{n},\rho} = \sigma^2_{\text{n}} + \sigma^2_{\text{I},\rho}$ is a combination of the noise variance in (4) and the residual interference terms not considered in the adjacency matrix $\mathbf{A}$, controlled by ε. The interference power is assumed to be Gaussian distributed with variance

$$\sigma^2_{\text{I},\rho} = \sum_{[\mathbf{A}]_{\rho,i}=0} \sigma^2_{\text{d}} \left|\upsilon^{(\rho,i)}\right|^2 \quad . \tag{13}$$

Note, by choosing $\varepsilon = 0$ all possible symbols are connected to a factor leading to a huge amount of complexity but $\sigma^2_{\text{I}} = 0$. In contrast, the message from a variable node $D^{(\psi)}$ to a factor node $Y^{(\rho)}$ is the product of all incoming messages of all other connected factor nodes and is given by

$$\mu_{D^{(\psi)}\to Y^{(\rho)}}\left(d^{(\psi)}\right) = \mu_{\text{Dem}\to D^{(\psi)}}\left(d^{(\psi)}\right) \prod_{\sim\{d^{(\psi)}\}} \mu_{Y^{(\rho)}\to D^{(\psi)}}\left(d^{(\psi)}\right) . \tag{14}$$

Here, $\mu_{\text{Dem}\to D^{(\psi)}}\left(d^{(\psi)}\right)$ is the a-priori message coming from the demodulator of the factor graph. The message from the equalizer to the demodulator is given by

$$\mu_{D^{(\psi)}\to\text{Dem}}\left(d^{(\psi)}\right) = \prod_{\psi} \mu_{Y^{(\rho)}\to D^{(\psi)}}\left(d^{(\psi)}\right) \tag{15}$$

The procedure of the SPA is shown in Alg. 1. The factor graph is initialized based on the adjacency matrix $\mathbf{A}$ from (8), particularly on ε. Usually this kind of factor graph has loops between neighboring variables and factors [19], hence the messages can not be calculated directly and an iterative calculation should be done. Thus, in lines 3 and 4 of Alg. 1 the messages are initialized as equally distributed.

Alg. 1 SPA Equalizer

#Initialize factor graph # setup the edges based on the adjacency matrix like in (8)
#Initialize#
$\mu_{Y^{(\rho)}\to D^{(\psi)}}\left(d^{(\psi)}\right) = 1/M$
$\mu_{D^{(\psi)}\to Y^{(\rho)}}\left(d^{(\psi)}\right) = 1/M$
repeat
  #Calculate variable to factor message#
  for $\psi = 0, \psi \leq N_k N_\ell - 1, \psi = \psi + 1$ **do**
    calculate $\mu_{D^{(\psi)}\to Y^{(\rho)}}\left(d^{(\psi)}\right)$ like in (14)
  end for
  #Calculate factor to variable message#
  for $\rho = 0, \rho \leq N_k N_\ell - 1, \rho = \rho + 1$ **do**
    calculate $\mu_{Y^{(\rho)}\to D^{(\psi)}}\left(d^{(\psi)}\right)$ like in (11) and (12)
  end for
until Any stopping criterion is met
#calculate equalizer output message#
calculate $\mu_{D^{(\psi)}\to \text{Dem}}\left(d^{(\psi)}\right)$ like in (15)

The amount of messages exchanged within the factor graph of the equalizer depends mainly on the number of iterations N_{it} and number of edges given by

$$N_{\mu,\text{exchanged}} = N_{\text{it}} \sum_{\psi=0}^{N_k N_\ell - 1} N_{\text{edges}}^{(d)}(\psi) = N_{\text{it}} \sum_{\rho=0}^{N_k N_\ell - 1} N_{\text{edges}}^{(y)}(\rho) \quad (16)$$

and gives a first indication on the complexity of the calculation of the SPA. Furthermore, the complexity of the messages depends on their possible implementations, e.g., probability domain, log domain or Log-Likelihood Ratio (LLR) domain and the system model. However, the calculation of the messages also scale with the number of edges per node and the modulation alphabet. By assuming the calculation in the probability domain and the same number of edges for simplicity like $N_{\text{edges}}^{(d)}(\psi) = N_{\text{edges}}^{(y)}(\rho)$ omitting the indices, the number of additions per message are given by

$$N_{\text{Additions,per Message}} = \frac{1}{2}\left(N_{\text{edges}} 2^{N_{\text{edges}}}\right)\left(M \log_2(M)\right), \quad (17)$$

likewise, the number of multiplications per message is:

$$N_{\text{Multiplications,per Message}} = \left(2N_{\text{edges}} 2^{N_{\text{edges}}}\right)\left(M \log_2(M)\right) + \left(N_{\text{edges}} - 1\right)\log_2(M). \quad (18)$$

The complexity grows linearly with the number of iterations N_{it} and the number of resources N_k or N_ℓ within the multi-carrier scheme as shown in (16). However, the main impact is given by the modulation alphabet scaling with $M\log_2(M)$ and the number of edges scaling with $2N_{\text{edges}}2^{N_{\text{edges}}}$, which is mainly dominated by the channel and the waveform and controlled by the threshold ε in (8).

D. Performance in P2P Transmission

For performance evaluation, multi-carrier systems with BPSK modulation are considered, where $N_{\text{h}} = 50$ complex Rayleigh fading coefficients h_ι with $\iota = 0, \ldots, N_{\text{h}} - 1$ are assumed. The time delay spread τ_ι and the Doppler shift ν_ι are equally distributed within $[0, \tau_{\max}]$ and $[-\nu_{\max}, \nu_{\max}]$, respectively. In total, $N_k = 32$ sub-carriers and $N_\ell = 20$ time symbols are used to generate a frame containing 640 data symbols, thus, the matrix $\mathbf{V}$ contains 409,600 elements. As the complexity of the SPA is mainly controlled by the threshold ε in (8), we choose the threshold ε such, that each row in $\mathbf{A}$ has N_{N} entries with one, i.e., only N_{N} symbols with the largest channel coefficient $\left|v^{(\rho,\psi)}\right|^2$ are considered in the factor graph keeping the complexity manageable. This leads to a factor graph with a constant number of edges $N_{\text{edges}} = N_{\text{N}}$ per node. Subsequently, we focus on the following combination of multi-carrier schemes and equalizers:

1) CP-OFDM with 1-tap equalizer or SPA equalizer
2) OFDM with 1-tap equalizer or SPA equalizer
3) QAM/FBMC with SPA equalizer

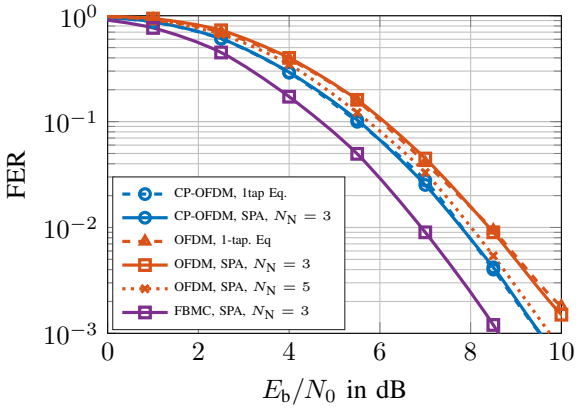

Fig. 4. FER analysis with different multi-carrier schemes applying 1-tap Eq. (dashed), factor graph based Eq. with $N_{\text{N}} = 3$ (solid) and $N_{\text{N}} = 5$ (dotted) affected by time-invariant channel.

Fig. 4 shows the FER performance at the receiver with the different schemes. The channel is assumed to be a block fading channel with a delay spread of $\Delta\tau_{\max} = 0.2T$. The guard interval of the CP-OFDM schemes have the same length than the delay spread. We can observe that CP-OFDM with 1-tap and SPA achieve the same performance, due to the fully diagonal structure of the effective channel (see Fig. 3). The performance of OFDM without a CP decreases due to the additional Inter-Symbol Interference (ISI), which cannot be fully utilized by the SPA using only a few neighboring symbols $N_{\text{N}} = 3$. However, considering more useful power in the factor graph with $N_{\text{N}} = 5$ the FER performance increases to the CP-OFDM case. On the contrary, QAM/FBMC with only $N_{\text{N}} = 3$ outperforms all other schemes exploiting the well-localized property of the Gaussian waveform without the loss of an additional guard interval.

An additional CFO of $\Delta\nu = 0.2F$ is added to the channel and the FER performance is shown in Fig. 5. Within this scenario the useful power is spread over the available bandwidth as indicated in Fig. 3. Applying 1-tap equalization to OFDM leads to a catastrophic performance degradation

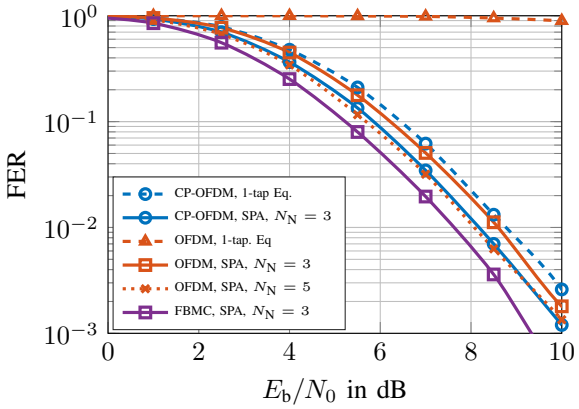

Fig. 5. FER analysis, with different multi-carrier schemes applying 1-tap Eq. (dashed) and factor graph based Eq. with $N_N = 3$ (solid) and $N_N = 5$ (dotted) affected by time-invariant channel and an additional CFO.

due to the huge amount of interference without a CP and additional Inter-Carrier Interference (ICI). The CP-OFDM using 1-tap equalization decreases in performance compared to the previous case, whereas CP-OFDM with SPA and $N_N = 3$ achieves almost the same performance. Here, OFDM applying $N_N = 3$ and $N_N = 5$ outperforms both CP-OFDM schemes. QAM/FBMC utilizes more useful power and outperforms again all other schemes.

The FER performance regarding a different number of neighbors N_N in the factor graph and a different number of iterations within the equalizer is analyzed in Fig. 6. The channel is assumed to be double-dispersive with $\Delta\tau = 0.2T$ and $\Delta\nu = 0.2F$ and no additional offsets at a working point of E_b/N_0 with 4.5dB. All three schemes are compared to the following cases

1) *No a-priori* information available (equally distributed messages $\mu_{\text{Dem}\to D^{(\psi)}}\left(d^{(\psi)}\right)$ in (14)). No iterations between equalizer, demodulator and decoder. This is the worst case scenario and the lower bound of the achievable FER performance.
2) *Perfect a-priori* information at the equalizer, which is the upper bound of this setting.

It can be observed in Fig. 6(a) that with only applying one edge $N_N = 1$ in the factor graph (or in other words 1-tap equalization) CP-OFDM outperforms all other schemes, due to the inherent robustness to ISI by the CP. The other schemes suffer from huge amount of interference, not considered in the factor graph. Even with perfect a-priori information the SPA cannot exploit this knowledge and, thus, no gain is achieved. In contrast, allowing more edges, all schemes achieve an increased FER performance at the cost of higher complexity as indicated above. However, the highest performance-enhancement is achieved by the QAM/FBMC scheme. The well-localized Tx/Rx filters lead to a small spreading over the time-frequency grid which can be exploited by the SPA in the equalizer. Even without any a-priori information the FBMC outperforms all other schemes considering $N_N \geq 4$. Fig. 6(b) shows the FER performance of all schemes regarding

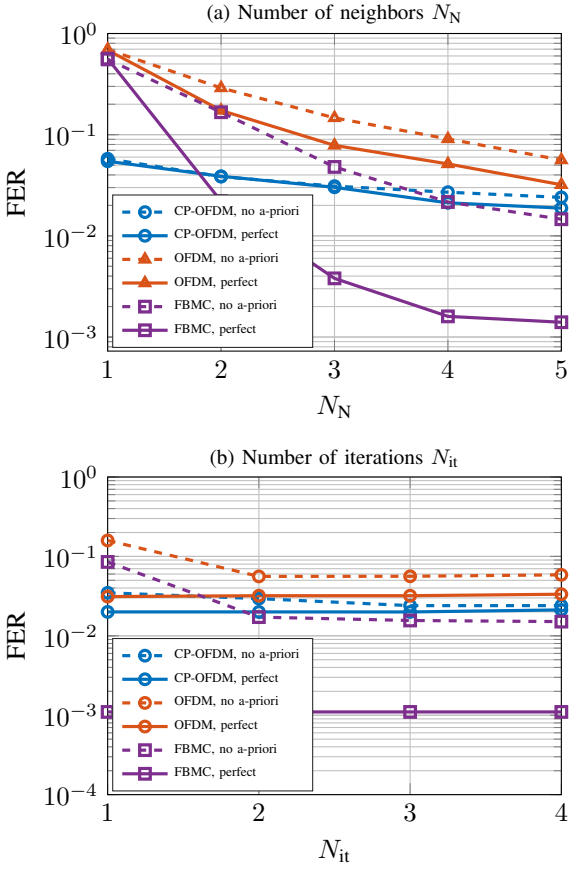

Fig. 6. FER analysis with (a) different N_N, $N_{it} = 3$ and (b) different N_{it}, $N_N = 3$ under time-variant channel $\tau_{max} = 0.2T$ and $\nu_{max} = 0.2F$.

the number of iterations within the equalizer. All schemes have no further improvement with $N_{it} \geq 2$. With perfect a-priori information no improvement is achieved due to perfect message available after the first iteration.

III. TWRC Transmission

In two-phase TWRC the exchange of information between two users is assisted by an intermediate relay. In the Multiple Access Channel (MAC) phase both user data streams $\mathbf{d}_A$ and $\mathbf{d}_B$ are transmitted over individual channels $\mathbf{V}_A$ and $\mathbf{V}_B$ to the relay R. Important to note is that both users have to use the same linear encoding scheme and modulation scheme. The superposition

$$\mathbf{y}_R = \mathbf{V}_A\mathbf{d}_A + \mathbf{V}_B\mathbf{d}_B + \mathbf{n}_R \tag{19}$$

is received at the relay. The corresponding factor graph generating (19) is illustrated in Fig. 7. The adjacency matrix can be calculated for each user individually like in (8) yielding matrices $\mathbf{A}_A$ and $\mathbf{A}_B$. In the broadcast phase one combined data signal vector $\mathbf{d}_R$ is transmitted to both users. Each user estimates the corresponding information sequence $\mathbf{b}_R = \mathbf{b}_A \oplus \mathbf{b}_B$, which is the bitwise XORed combination of both user information sequences. Thus, both users can estimate the information sequence of the other user, because they are

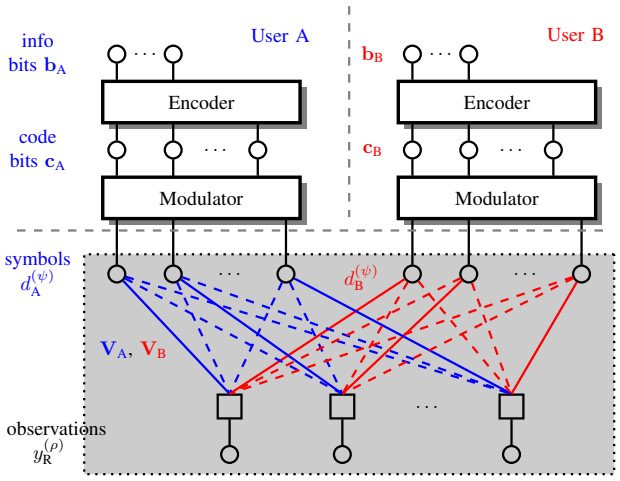

Fig. 7. Factor graph of the MAC phase. Edges between the symbol variable of user A and channel observations in red, for user B in blue.

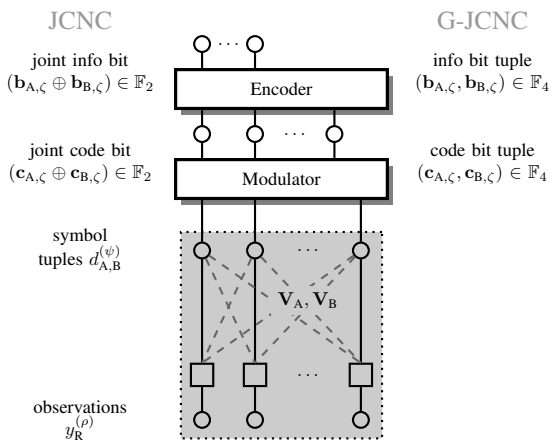

Fig. 8. Factor graph for the JCNC schemes. Notation for JCNC on the left side, G-JCNC on the right side.

aware of their own message. The task at the relay is to generate this combined data signal vector $\mathbf{d}_\mathrm{R}$ based on the received signal vector $\mathbf{y}_\mathrm{R}$. The challenge is the superposition of both users affected by their individual channels $\mathbf{V}_\mathrm{A}$ and $\mathbf{V}_\mathrm{B}$ at the relay.

In contrast to the P2P user case, where the impact of, e.g., CFO and TO can be significantly reduced by compensation algorithms, the effects can not be compensated, even if the impact is perfectly known [13]. To reduce the offsets an average compensation is proposed in [24]. Subsequently, we assume that an average compensation strategy is already applied, and only the residual terms are present. Hence, an equalizer is needed, dealing with these residual effects.

A. Equalization and Detection

Within the TWRC different detection schemes were proposed [3] and [6] like separate detection of each user information $\mathbf{b}_\mathrm{A}$ and $\mathbf{b}_\mathrm{B}$ or joint detection of either a user tuple $(\mathbf{b}_\mathrm{A}, \mathbf{b}_\mathrm{B})$ or a combined message $\mathbf{b}_\mathrm{R}$ directly used in the broadcast phase.

1) Generalized Joint Channel Decoding and Physical-Layer Network Coding (JCNC): The G-JCNC detection scheme estimates the ζ^{th} joint bit tuple $(b_{\mathrm{A},\zeta}, b_{\mathrm{B},\zeta}) \in \mathbb{F}_4$ and after detection performs a bitwise XOR operation to generate the combined information sequence $\mathbf{b}_\mathrm{R} = \mathbf{b}_\mathrm{A} \oplus \mathbf{b}_\mathrm{B}$ for the broadcast phase. The MAP detector for the G-JCNC becomes

$$(\tilde{b}_{\mathrm{A},\zeta}, \tilde{b}_{\mathrm{B},\zeta}) = \underset{(b_{\mathrm{A},\zeta}, b_{\mathrm{B},\zeta}) \in \mathbb{F}_4}{\arg\max}\; p\left((b_{\mathrm{A},\zeta}, b_{\mathrm{B},\zeta})|\mathbf{y}\right). \tag{20}$$

The pairing of bit tuples leads directly to a symbol vector tuple $\mathbf{d}_\mathrm{A,B} = (\mathbf{d}_\mathrm{A}, \mathbf{d}_\mathrm{B})$, thus, the messages in (11), (14) and (15) change to two-dimensional message $\mu_{Y^{(\rho)} \to D_\mathrm{A,B}^{(\psi)}}\left(d_\mathrm{A,B}^{(\psi)}\right)$, $\mu_{D_\mathrm{A,B}^{(\psi)} \to Y^{(\rho)}}\left(d_\mathrm{A,B}^{(\psi)}\right)$ and $\mu_{D_\mathrm{A,B}^{(\psi)} \to \mathrm{Dem}}\left(d_\mathrm{A,B}^{(\psi)}\right)$ with the symbol tuple $d_\mathrm{A,B}^{(\psi)} = \left(d_\mathrm{A}^{(\psi)}, d_\mathrm{B}^{(\psi)}\right)$. The calculation of the likelihood function is also extended to symbol tuples given by (21) on the next page with effective noise power $\tilde{\sigma}_{\mathrm{n},\rho}^2 = \sigma_\mathrm{n}^2 + \sigma_{\mathrm{I,A},\rho}^2 + \sigma_{\mathrm{I,B},\rho}^2$ calculated according to (13). The joint detection of bit tuples leads to a modified factor graph shown in Fig. 8. Furthermore, the modulation and encoder block in the factor graph have to work with the representation of tuples yielding an increased complexity. In [6] a modulator and encoder SPA is presented working directly on the message to the demodulator $\mu_{D_\mathrm{A,B}^{(\psi)} \to \mathrm{Dem}}\left(d_\mathrm{A,B}^{(\psi)}\right)$. The SPA algorithm in Alg. 1 can be easily adapted for the TWRC case by changing the equations of the likelihood function by (21) and using $\mathbf{A}_\mathrm{A}$ and $\mathbf{A}_\mathrm{B}$.

2) Joint Channel Decoding and Physical-Layer Network Coding: A special case of G-JCNC is JCNC estimating directly the XORed combination $\mathbf{b}_\oplus = \mathbf{b}_\mathrm{A} \oplus \mathbf{b}_\mathrm{B}$, which simplifies the calculation at the relay for the modulator and encoder. The MAP detector simplifies to a single bit detection and reads

$$\tilde{b}_{\oplus,\zeta} = \arg\max_{b_{\oplus,\zeta} \in \mathbb{F}_2} p\left(b_{\oplus,\zeta}|\mathbf{y}\right). \tag{22}$$

The message to the demodulator can be calculated with $\mu_{D_\mathrm{A,B}^{(\psi)} \to Y^{(\rho)}}\left(d_\mathrm{A,B}^{(\psi)}\right)$ of the G-JCNC detector and is given by

$$\mu_{D_\mathrm{A,B}^{(\psi)} \to \mathrm{Dem}}\left(\mathcal{M}\left(\mathbf{c}'_\mathrm{R} = \gamma\right)\right) = \sum_{\mathbf{c}'_\mathrm{A} \oplus \mathbf{c}'_\mathrm{B} = \gamma} \mu_{D_\mathrm{A,B}^{(\psi)} \to \mathrm{Dem}}\left(\left(\mathcal{M}\left(\mathbf{c}'_\mathrm{A}\right), \mathcal{M}\left(\mathbf{c}'_\mathrm{B}\right)\right)\right). \tag{23}$$

Each code vector $\mathbf{c}'$ contains the $\log_2(M)$ corresponding bits used by the modulator $\mathcal{M}(\cdot)$ and $\gamma = 0, \ldots, \log_2(M)$ is the corresponding decimal numbering of $\mathbf{c}'$. Hence, the detection scheme directly works on the relay message $\mathbf{c}_\mathrm{R} = \mathbf{c}_\oplus$. The factor graph is the same like in Fig. 8 using a binary encoder and a modulator with single symbols.

3) Separate Channel Decoding (SCD): This detection scheme is based on the factor graph in Fig. 7, each user information sequence $\mathbf{b}_i$ with $i \in \{\mathrm{A}, \mathrm{B}\}$ is detected separately and combined after detection by the bitwise XOR operation $\mathbf{b}_\mathrm{R} = \mathbf{b}_\mathrm{A} \oplus \mathbf{b}_\mathrm{B}$. Therefore, the user-wise MAP detector changes to

$$\tilde{b}_{i,\zeta} = \arg\max_{b_{i,\zeta} \in \mathbb{F}_2} p\left(b_{i,\zeta}|\mathbf{y}\right) \quad , \tag{24}$$

$$p\left(y_{\mathrm{R}}^{(\rho)}, \mathbf{d}_{\mathrm{A,B}}\right) \propto \exp\left(-\frac{1}{\tilde{\sigma}_{\mathrm{n}}^2}\left|y_{\mathrm{R}}^{(\rho)} - \sum_{\psi} \upsilon_{\mathrm{A}}^{(\rho,\psi)} d_{\mathrm{A}}^{(\psi)} - \sum_{\psi} \upsilon_{\mathrm{B}}^{(\rho,\psi)} d_{\mathrm{B}}^{(\psi)}\right|^2\right). \tag{21}$$

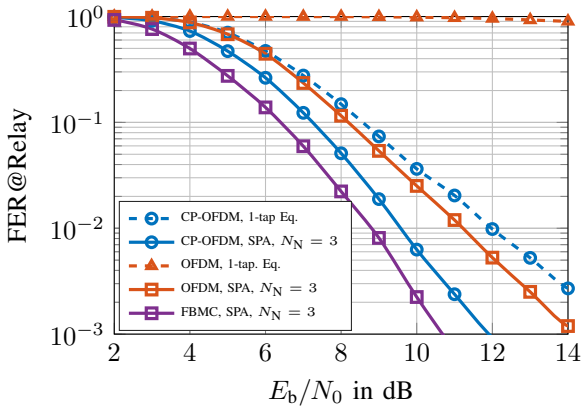

Fig. 9. FER performance of TWRC transmission applying the G-JCNC detector affected by time-invariant channel and individual CFO.

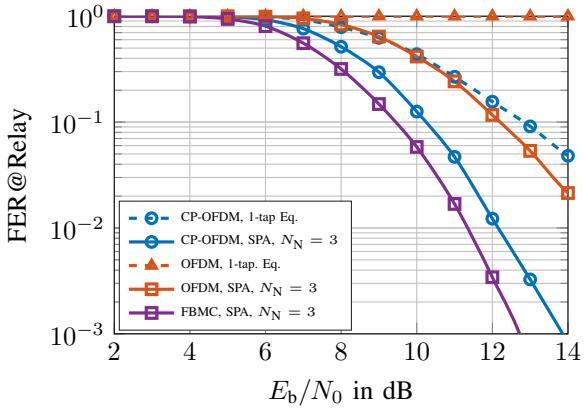

Fig. 10. FER performance of TWRC transmission applying the JCNC detector affected by time-invariant channel and individual CFO.

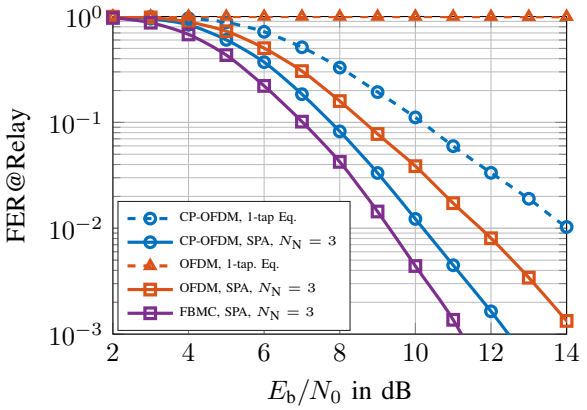

Fig. 11. FER performance of TWRC transmission applying the SCD detector affected by time-invariant channel and individual CFO.

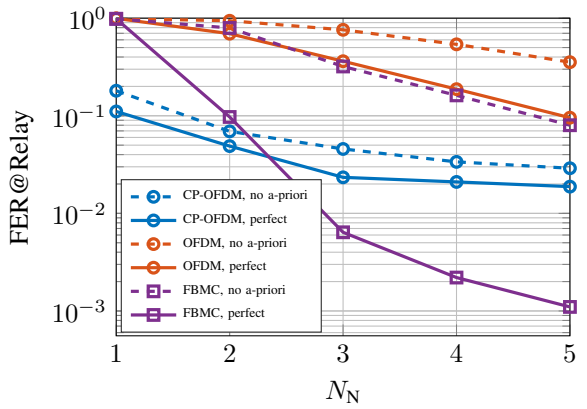

Fig. 12. FER performance with different number of edges in the factor graph applying the G-JCNC detector affected by time-variant channel.

The message from equalizer to the user A like in (15) is calculated separately by marginalization of the other user like

$$\mu_{D_{\mathrm{A,B}}^{(\psi)}\to\mathrm{Dem}}\left(\mathcal{M}\left(\mathbf{c}'_{\mathrm{A}}=\gamma\right)\right) = \sum_{\mathbf{c}'_{\mathrm{A}}=\gamma} \mu_{D_{\mathrm{A,B}}^{(\psi)}\to\mathrm{Dem}}\left(\left(\mathcal{M}\left(\mathbf{c}'_{\mathrm{A}}\right), \mathcal{M}\left(\mathbf{c}'_{\mathrm{B}}\right)\right)\right). \tag{25}$$

The message for the user B is calculated in the same way.

B. Performance Evaluation for TWRC Transmission

In this section, we consider TWRC where both users apply BPSK transmission to a relay with the same multi-carrier setting like in the P2P case. The channels are assumed to be time-invariant with a delay spread of $\tau_{\max} = 0.2T$ and an additional individual CFO of $\Delta\nu_{\mathrm{A}} = 0.2F$ and $\Delta\nu_{\mathrm{B}} = -0.2F$. Fig. 9 - 11 show the FER performance of the different detection schemes at the relay. In all three scheme, it can be observed that OFDM with 1-tap equalization suffers completely from the additional interference introduced by the channel. The CP-OFDM case with 1-tap equalization has significant degradations compared to the scheme applying the factor graph based equalizer which outperforms the 1-tap equalization scheme in all detection schemes by around 3dB or even more. Applying general waveform in FBMC further outperforms the other schemes by an additional gain of 1dB. Analyzing the FER performances w.r.t. the detection schemes show that G-JCNC outperforms all other schemes exploiting the message from the equalizer to the demodulator $\mu_{D_{\mathrm{A,B}}^{(\psi)}\to\mathrm{Dem}}$ completely in the factor graph. The SCD detection scheme performs slightly worse, the message is marginalized over the users and, thus, the information is not fully used in the factor graph. The JCNC scheme is outperformed by the both other schemes by roughly 2-3dB as also indicated in [12].

Fig. 12 shows the FER performance of G-JCNC w.r.t. the number of edges used per node in the factor graph at a working point of 5dB affected by a time-variant channel with $\tau_{\max} = 0.2T$ and $\nu_{\max} = 0.2F$. The slope of the FER performance of the OFDM systems indicates only small improvements by further incrementing the number of edges within the factor graph. In contrast to that, FBMC starts with a high improvement utilizing only a few edges in the factor graph. Similar to the P2P case in Fig. 6(a), FBMC outperforms all other schemes with the number of edges $N_{\mathrm{N}} \geq 3$ in the ideal case.

IV. Summary And Outlook

In this paper, we analyzed factor graph based equalization techniques for multi-carrier transmissions in TWRCs. The combination of waveforms and factor graphs outperforms the classical CP-OFDM with 1-tap equalization w.r.t the FER performance at the relay. Furthermore, it offers a flexible control over the complexity by utilizing only a reduced number of edges within the factor graph. Further investigations on the interaction of waveforms and factor graph equalizer will be done in the future.

V. Acknowledgment

This work was partly funded by the German Research Foundation (DFG) under grant WU 499/10-1 and by the German ministry of education and research (BMBF) under grant 16KIS0263K.

References

[1] G. Wunder, P. Jung, M. Kasparick, T. Wild, F. Schaich, Y. Chen, S. ten Brink, I. Gaspar, N. Michailow, A. Festag, L. Mendes, N. Cassiau, D. Ktnas, M. Dryjanski, S. Pietrzyk, B. Eged, P. Vago, and F. Wiedmann, "5GNOW: Non-Orthogonal, Asynchronous Waveforms for Future Mobile Applications," *Communications Magazine, IEEE*, vol. 52, no. 2, Feb. 2014.

[2] M. Bellanger, "Physical layer for future broadband radio systems," in *Radio and Wireless Symposium (RWS)*, Jan. 2010, pp. 436–439.

[3] S. Zhang, S.C. Liew, and P.P. Lam, "Hot Topic: Physical-layer Network Coding," in *12th annual International Conference on Mobile Computing and Networking (MobiCom 06)*, Los Angeles, CA, USA, 2006.

[4] S. Zhang, S.C. Liew, and P.P. Lam, "On the Synchronization of Physical-Layer Network Coding," in *IEEE Information Theory Workshop (ITW '06)*, Chengdu, China, Oct 2006, pp. 404–408.

[5] P. Popovski and H. Yomo, "Physical Network Coding in Two-Way Wireless Relay Channels," in *IEEE International Conference on Communications (ICC' 07)*, Glasgow, GB, June 2007.

[6] D. Wübben and Y. Lang, "Generalized Sum-Product Algorithm for Joint Channel Decoding and Physical-Layer Network Coding in Two-Way Relay Systems," in *2010 IEEE Global Telecommunications Conference GLOBECOM 2010*, Miami, Fl, USA, Dec. 2010, IEEE.

[7] D. Wübben, "Joint Channel Decoding and Physical-Layer Network Coding in Two-Way QPSK Relay Systems by a Generalized Sum-Product Algorithm," in *Communication Systems (ISWCS), 2010 7th*, York, Great Britain, Sept. 2010.

[8] C. K. Ho, R. Zhang, and Y.-C. Liang, "Two-Way Relaying over OFDM: Optimized Tone Permutation and Power Allocation," in *IEEE International Conference on Communications (ICC' 08)*, Bejing, China, 2008.

[9] B. Han, W. Wang, and M. Peng, "Optimal Resource Allocation for Network Coding in Multiple Two-Way Relay OFDM Systems," in *IEEE Wireless Communications and Networking Conference (WCNC 12)*, Paris, France, April 2012.

[10] Jie Huang and Shengli Zhou, "Turbo Equalization for OFDM modulated Physical Layer Network Coding," *2011 IEEE 12th International Workshop on Signal Processing Advances in Wireless Communications*, pp. 291–295, Jun. 2011.

[11] I. W.-H. Ho, S.C. Liew, and L. Lu, "Feasibility Study of Physical-Layer Network Coding in 802.11p VANETs," in *IEEE International Symposium on Information Theory (ISIT' 14) 2014*, Honolulu, HI, USA, June 2014.

[12] M. Wu, D. Wübben, and A. Dekorsy, "Mutual Information Based Analysis for Physical-Layer Network Coding with Optimal Phase Control," in *9th International ITG Conference on Systems, Communications and Coding (SCC' 13)*, Munich, Germany, Jan. 2013.

[13] M. Wu, F. Ludwig, M. Woltering, D. Wübben, A. Dekorsy, and S. Paul, "Analysis and Implementation for Physical-Layer Network Coding with Carrier Frequency Offset," in *International ITG Workshop on Smart Antennas (WSA2014)*, Erlangen, Germany, Mar 2014.

[14] M. Woltering, D. Wübben, and A. Dekorsy, "Comparison of General Multi-Carrier Schemes in Two Way Relaying Channels," in *20th International ITG Workshop on Smart Antennas (WSA'2016)*, Munchich, Germany, Mar. 2016.

[15] F. R. Kschischang, B. J. Frey, and H.-A. Loeliger, "Factor Graphs and Sum Product Algorithm," *IEEE Transactions on Information Theory*, vol. 47, no. 2, pp. 498–519, 2001.

[16] H.-A. Loeliger, "An Introduction to Factor Graphs," *IEEE Signal Processing Magazine*, vol. 21, no. 1, pp. 28–41, Jan. 2004.

[17] H. Wymeersch, *Iterative Receiver Design*, Cambridge University Press, 2007.

[18] P. Ochandiano, H. Wymeersch, M. Mendicute, L. Martínez, and I. Sobrón, "Factor Graph based Detection Approach for High-Mobility OFDM Systems with large FFT Modes," *EURASIP Journal on Wireless Communications and Networking*, vol. 2012, no. 1, pp. 1–12, 2012.

[19] Xiang Xu and Rudolf Mathar, "Factor Graph based Detection and Channel Estimation for MIMO-OFDM systems in Doubly Selective Channel," *Proceedings of the 2010 7th International Symposium on Wireless Communication Systems, ISWCS'10*, pp. 456–460, sep 2010.

[20] S. Schedler, M. Woltering, D. Wübben, V. Kühn, and A. Dekorsy, "Investigation on Gaussian Waveforms to Improve Robustness in Physical Layer Network Coding," in *18th International OFDM Workshop 2014 (InOWo'14)*, Essen, Germany, Aug. 2014.

[21] M. Woltering, D. Wübben, A. Dekorsy, S. Schedler, and V. Kühn, "Physical Layer Network Coding Using Gaussian Waveforms: A Link Level Performance Analysis," in *10th International ITG Conference on Systems, Communications and Coding (SCC'15)*, Hamburg, Germany, Feb 2015.

[22] M. Woltering, D. Wübben, and A. Dekorsy, "Physical Layer Network Coding with Gaussian Waveforms using Soft Interference Cancellation," in *IEEE 81th Vehicular Technology Conference (VTC2015-Spring)*, Glasgow, Great Britain, May 2015.

[23] H.-A. Loeliger, "Some Remarks on Factor Graphs," *Proc. 3rd International Symposium on Turbo Codes and Related Topics*, , no. 3, pp. 1–5, 2003.

[24] L. Lu, T. Wang, S. C. Liew, and S. Zhang, "Implementation of Physical-Layer Network Coding," *Physical Communication*, vol. 6, pp. 74–87, Mar. 2013.